# Research On Robot Intelligent Delivery Based On Adaptive CLAHE-LAB Spatial Feature Fusion Algorithm

Jinyu Ren, Weijie Ma, and Qi Yang*

School of Mechanical Engineering, Shenyang Ligong University, Shenyang, Liaoning, China

*Corresponding author. E-mail: yangqi@sylu.edu.cn

Received: June 2, 2026; Accepted: June 28, 2026

To address illumination-induced color recognition instability, ball stacking and jamming during continuous delivery, and reduced reliability of intelligent delivery robots in complex environments, this paper proposes a robot intelligent delivery method integrating an anti-jamming storage structure and an adaptive CLAHE-LAB spatial feature fusion algorithm. First, a passive anti-jamming ball storage structure based on ball-diameter constraints is designed for continuous ball storage and delivery. A top light shield reduces external illumination interference, a ball-diameter-matched multi-hole inlet array disperses the ball entry path, and inner-wall antibridging limiting ribs disrupt stable support states caused by multi-ball stacking, thereby reducing the risk of jamming and discharge interruption. Second, an adaptive CLAHE-LAB spatial feature fusion algorithm is proposed to overcome false and missed detection caused by traditional RGB/HSV threshold segmentation under weak, strong, and non-uniform illumination. By decoupling luminance and chromaticity in LAB space, enhancing local contrast, and fusing color saliency features, the separability between blue targets and the background is improved. Finally, an experimental platform is built to evaluate color recognition, segmentation accuracy, jamming frequency, and continuous delivery success rate. Experimental results show that the proposed method improves blue target recognition stability, alleviates ball stacking and jamming, and enhances continuous delivery reliability.

**Keywords:** Intelligent delivery robot; Adaptive CLAHE; LAB color space; Feature fusion; Color recognition

http://dx.doi.org/10.6180/jase.202611_34.039

## 1. Introduction

With the development of mobile robots, machine vision, and embedded control technologies, small intelligent delivery robots for sorting, transportation, competition, and service scenarios have attracted increasing attention. Existing studies have combined machine vision with robotic actuators for object classification, material sorting, and robotic grasping control [1, 2], and have further extended these techniques to industrial sorting, multi-category waste recognition, color-object sorting, and vision-based sorting robots [3–6]. For robots that deliver spherical objects, the system must not only perform color recognition and target localization, but also ensure the continuity of ball storage, discharge, and delivery actions. Therefore, visual robustness, storage stability, and actuator coordination jointly determine the overall performance and engineering applicability of an intelligent delivery robot.

Existing color recognition methods mainly include RGB threshold segmentation, HSV color-space segmentation, image enhancement preprocessing, and multi-color-space fusion. RGB thresholding is computationally simple and easy to deploy, but color and brightness information are strongly coupled, making thresholds prone to drift under weak light, strong light, or local reflection. The HSV space improves color representation and has been applied to color image segmentation [7, 8], while the LAB color space separates luminance from chromaticity and can reduce the influence of illumination changes on color feature extraction [9–11]. In addition, adaptive histogram equalization and its variants can enhance local contrast [12]. Recent studies on low-light and non-uniform illumination enhancement show that brightness-adaptive enhancement is helpful for improving target separability in dark, shadowed, and reflective scenes [13, 14]. Other studies further improve low-light image quality through filtering enhancement, Retinex modeling, ultra-high-definition enhancement, signal-to-noise-ratio awareness, and fast robust enhancement strategies [15–18]. Related feature fusion methods also improve the stability of low-light image enhancement [19–21]. These studies provide useful references for color target recognition under complex illumination. However, in embedded robot scenarios, algorithms must still balance recognition stability, computational complexity, parameter adaptivity, and real-time deployment requirements.

In addition to visual recognition, mechanical reliability during continuous multi-ball delivery also affects system performance. When multiple balls enter the storage bin simultaneously, random contact and local extrusion occur among the balls. Constrained by bin size, inlet position, ball diameter, and the discharge channel, balls may form stacking, bridging, or arching states, resulting in uneven discharge intervals, delivery interruption, or complete jamming. Studies on granular flow and silo clogging show that obstacles and structural constraints can change granular discharge states and affect clogging probability [22]. The arch-like contact structures formed before discharge are also directly related to hopper clogging [23]. For small robots with limited space, relying only on additional actuators or complex control logic to solve ball jamming often increases system weight, manufacturing cost, and control difficulty. Therefore, passive structural design that improves the ball entry path and the contact state inside the bin is an effective approach for improving continuous delivery reliability.

In summary, although many achievements have been made in color recognition algorithms, image enhancement, and robotic sorting systems, two limitations remain for small intelligent delivery robots. First, traditional color segmentation methods mostly rely on a single color space or fixed thresholds, which are not sufficiently adaptive to complex illumination, local reflection, and shadow interference, and may cause missing target edges, background false detection, and center localization deviation. Second, some delivery structures focus more on actuator motion while paying insufficient attention to random multi-ball stacking, bridging, and jamming inside the storage bin, which may cause discharge interruption or delivery failure during continuous operation.

To address these problems, this paper proposes a robot intelligent delivery method that integrates an anti-jamming storage structure with an adaptive CLAHE-LAB spatial feature fusion algorithm. The main contribution is that a passive anti-jamming ball storage structure based on ball-diameter constraints is designed to disperse the ball entry path and disrupt stable multi-ball support states through a top light shield, a multi-hole inlet array, and inner-wall limiting ribs, while an adaptive CLAHE-LAB feature fusion algorithm is developed to construct blue response features and adaptively adjust enhancement parameters and segmentation thresholds according to brightness statistics. Through the collaboration of structural disturbance reduction and visual enhancement, the proposed method improves blue target recognition stability and continuous delivery reliability under complex illumination conditions.

## 2. System design

### 2.1. System Composition and Working Process

The robot intelligent delivery system mainly consists of a mobile chassis, a ball storage bin, an anti-jamming delivery structure, a visual recognition module, a control module, and actuators. The visual module captures images of the target area, and the adaptive CLAHE-LAB spatial feature fusion algorithm is used to complete color recognition and target localization. According to the recognition result, the control module drives the corresponding actuator to complete the sorting or delivery action.

During operation, the robot first moves to the material storage area, where balls enter the storage bin through the anti-jamming structure. The structure constrains the ball entry path and reduces unstable stacking inside the bin. After image acquisition and color recognition, the controller outputs delivery commands, and the delivery mechanism unloads the target balls and returns to the initial state for the next cycle. The exploded structure and physical prototype of the robot intelligent delivery system are shown in Fig. 1.

### 2.2. Hardware design of the control system

The control system consists of a main control unit, a visual acquisition module, motor/servo driving modules, a power supply module, and communication interfaces. The visual module is responsible for collecting ball images, while the main control unit performs recognition-result parsing, delivery logic judgment, and actuator control. After the target color and center coordinates are obtained,

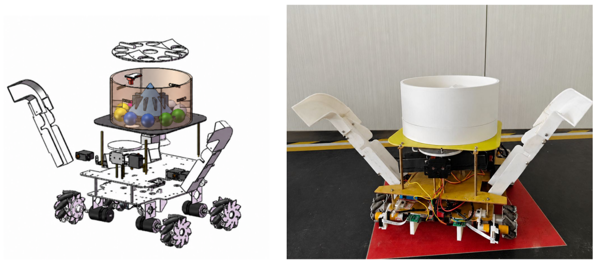

**Fig. 1.** Exploded structure and physical prototype of the robot intelligent delivery system.

the controller converts the recognition result into a delivery command and drives the servo actuator to complete unloading at the corresponding position.

In this control framework, the visual module and the actuator module are connected through a simple sequential logic. The visual module first completes image acquisition and color judgment, and the controller then determines whether the current recognition result satisfies the delivery condition. When the target is confirmed, the corresponding servo action is triggered according to the preset delivery state; otherwise, the mechanism remains in the waiting state and continues to receive visual feedback. This design keeps the control process lightweight and helps coordinate recognition, decision-making, and unloading within one delivery cycle.

The hardware design also emphasizes modular connection and stable signal transmission. The visual acquisition module provides target information, the main control unit performs task-state judgment, and the motor/servo driving modules execute movement and unloading commands. The power supply module provides independent support for the controller and actuators to reduce interference caused by instantaneous motor current changes. Through this modular organization, the recognition module, control module, and delivery mechanism can operate in a coordinated manner while keeping the system structure simple and suitable for compact robot platforms. The hardware connection relationship is shown in Fig. 2.

### 2.3. Anti-jamming ball storage structure design based on ball-diameter constraints

#### *2.3.1. Analysis of ball-bin jamming*

During continuous multi-ball delivery, balls in the storage bin experience extrusion and random contact. Near the limited discharge channel, multiple balls may form stacking, bridging, or arching states among the bin wall, bottom plate, and adjacent balls, resulting in uneven discharge intervals, delivery interruption, or complete jamming.

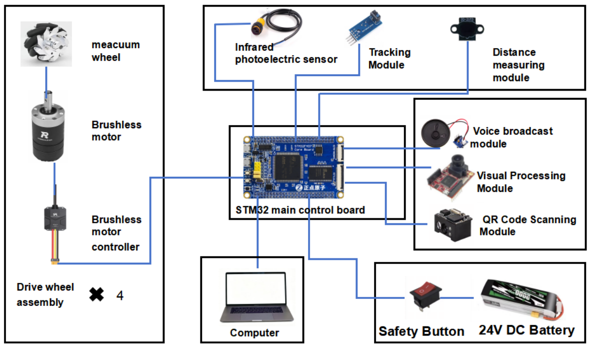


**Fig. 2.** Circuit design of the control system.

Mechanically, jamming can be regarded as a static equilibrium state under gravity, normal support forces, and friction. Let the gravity acting on the $i$th ball be $G_i$, the normal force be $N_{ij}$, and the friction force be $f_{ij}$. The local equilibrium can be approximated as

$$G_i + \sum_j N_{ij} + \sum_j f_{ij} = 0, \qquad f_{ij} \le \mu N_{ij}. \tag{1}$$

where $\mu$ is the contact friction coefficient. Therefore, anti-jamming design should reduce concentrated stacking and disrupt stable force-equilibrium conditions among balls.

#### *2.3.2. Multi-hole dispersed inlet and light-shielding structure design*

To reduce local accumulation, a ball-diameter-matched multi-hole inlet array is arranged at the top of the storage bin. Let the ball diameter be $D_b = 42\,\text{mm}$. This value is determined by the actual experimental ball specification, and the structural dimensions are selected around this diameter to ensure that the storage and discharge process remains consistent with the physical target. The inlet hole diameter is designed as

$$D_h = D_b + \Delta D_b, \tag{2}$$

where $D_h$ is the inlet hole diameter and $\Delta d$ is the motion clearance for smooth passage. The clearance is introduced to tolerate manufacturing error, ball surface roughness, and small pose deviations during entry; however, it should not be excessively large, otherwise multiple balls may enter the same local area at the same time and weaken the dispersion effect. Compared with a single large opening, the multi-hole inlet array disperses ball entry paths. If $n$ inlet holes are arranged, the average number of balls entering each inlet region can be approximated as

$$\bar{Q}_k = \frac{Q}{n}, \qquad k = 1, 2, \ldots, n. \tag{3}$$

where $Q$ is the total ball input per unit time. Thus, the multi-hole structure reduces instantaneous local concentration and decreases the probability of stacking and bridging.

This structure also works as a light shield for the recognition area, reducing direct external light, highlights, shadows, and background reflection. Together with the adaptive CLAHE-LAB algorithm, it forms a collaborative structural disturbance reduction and visual enhancement scheme.

#### 2.3.3. *Inner-wall anti-bridging limiting rib design*

Although the multi-hole inlet reduces concentrated entry, stable bridges may still form above the discharge area. Therefore, anti-bridging limiting ribs are arranged on the inner wall to disturb the support state during the transition from single-layer arrangement to double-layer stacking.

For balls with diameter $D_b$, when an upper ball is supported by two lower balls, its geometric center height $H_2$ can be approximated as

$$H_2 = \left(1 + \frac{\sqrt{3}}{2}\right) D_b. \tag{4}$$

Since $D_b < H_2 < 2D_b$, this interval corresponds to the typical transition region from single-layer rolling to double-layer stacking. Therefore, the limiting rib height is set as

$$h_r \in [D_b, H_2], \tag{5}$$

where $h_r$ is the height from the storage-bin bottom to the lower edge of the rib. Within this range, the rib changes ball-wall contact positions and angles, disrupts stable bridging, and promotes ball movement toward the discharge area. This height selection is therefore based on both the ball diameter constraint and the geometric stacking relationship, rather than being chosen empirically. The anti-jamming structure is shown in Fig. 3.

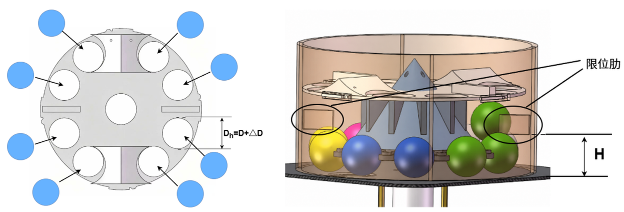


**Fig. 3.** Schematic diagram of the anti-jamming structure.

## 3. Adaptive clahe-lab feature fusion algorithm

### 3.1. Overall algorithm flow

To improve blue target recognition under complex illumination, this paper proposes an adaptive CLAHE-LAB spatial feature fusion algorithm. Its adaptivity is mainly reflected in two stages. In image enhancement, the CLAHE clip limit is calculated from the mean and standard deviation of the luminance channel to obtain the adaptive parameter $C_{\text{adp}}$, so that the enhancement intensity changes with illumination conditions. In target segmentation, the threshold is determined from the statistical distribution of the fused feature map to obtain $T_{\text{adp}}$, improving segmentation adaptability under different lighting conditions.

The robot system can recognize red, white, yellow, green, and blue balls. This paper takes the blue ball as a representative target because it is sensitive to illumination variation in the experimental background and can clearly reflect the robustness of the proposed feature-fusion strategy. Recognition of other colors can be achieved by modifying the corresponding color response feature while keeping the image enhancement, adaptive thresholding, and connected-component localization procedures unchanged.

The proposed algorithm first converts the RGB image into LAB space to separate luminance and chromaticity information, and then constructs the blue response feature from the $b$ channel. The blue feature is enhanced using adaptive CLAHE and fused with chromaticity and luminance constraint features. Finally, adaptive threshold segmentation, morphological processing, and connected-component analysis are used to obtain the target center coordinates. The flowchart of the proposed algorithm is shown in Fig. 4.

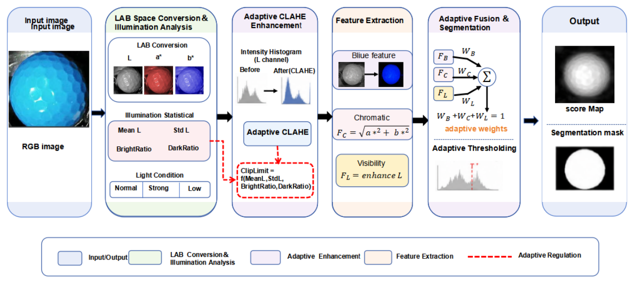


**Fig. 4.** Flowchart of the proposed algorithm.

### 3.2. LAB color-space conversion and blue response feature construction

Let the RGB image captured by the visual module be expressed as

$$I_{\text{RGB}}(x, y) = [R(x, y), G(x, y), B(x, y)], \tag{6}$$

where $(x, y)$ denotes the image pixel coordinate, and $R(x, y)$, $G(x, y)$, and $B(x, y)$ denote the pixel values of the red, green, and blue channels, respectively. Since color information and luminance information are strongly coupled in the RGB color space, the pixel values of the three color channels are simultaneously affected when environmental illumination changes, resulting in reduced stability of fixed-threshold segmentation. To reduce the influence of illumination variation on color recognition, the RGB image is converted into the LAB color space:

$$I_{\mathrm{LAB}}(x,y) = [L(x,y), a(x,y), b(x,y)], \tag{7}$$

where $L$ denotes the luminance channel, $a$ denotes the red-green chromatic component, and $b$ denotes the yellow-blue chromatic component. For blue targets, the color feature has an obvious response in the $b$ channel. Therefore, this paper constructs the blue response feature based on the $b$ channel.

For subsequent feature fusion, the $b$ channel is first normalized:

$$b_n(x,y) = \frac{b(x,y) - b_{\min}}{b_{\max} - b_{\min} + \varepsilon}, \qquad B_r(x,y) = 1 - b_n(x,y), \tag{8}$$

where $b_{\min}$ and $b_{\max}$ denote the minimum and maximum values of the $b$ channel, respectively, $\varepsilon$ is a small constant used to prevent division by zero, and $B_r$ denotes the blue response feature map. Since blue regions usually show low-value responses in the LAB $b$ channel, the inverse normalization form can highlight the blue target region and assign higher response values to target pixels.

### 3.3. Adaptive CLAHE enhancement based on luminance statistics

CLAHE can enhance local image contrast. However, traditional CLAHE usually adopts fixed parameters and lacks adaptability under different illumination conditions. In weak-light environments, insufficient enhancement may lead to blurred target boundaries, while in strong-light or reflective environments, excessive enhancement may amplify noise and highlight regions. Therefore, this paper adaptively adjusts the CLAHE enhancement parameters according to the luminance distribution of the image.

First, the mean and standard deviation of the luminance channel $L$ are calculated as

$$\begin{aligned} \mu_{\mathrm{L}} &= \frac{1}{HW}\sum_{x=1}^{W}\sum_{y=1}^{H} L(x,y) \\ \sigma_{\mathrm{L}} &= \sqrt{\frac{1}{HW}\sum_{x=1}^{W}\sum_{y=1}^{H} \left(L(x,y) - \mu_{\mathrm{L}}\right)^2} \end{aligned} \tag{9}$$

where $H$ and $W$ denote the height and width of the image, respectively, $\mu_L$ denotes the average image luminance, and $\sigma_L$ denotes the dispersion degree of the luminance distribution. When strong light, reflection, or shadows exist in the image, luminance variation is large and $\sigma_L$ is usually large. When the luminance distribution is relatively smooth, $\sigma_L$ is small. Therefore, $\sigma_L$ can be used to describe the luminance fluctuation of the current image.

To constrain the luminance fluctuation degree within a unified range, a normalized luminance fluctuation coefficient is introduced:

$$\eta_L = \frac{\sigma_L}{\mu_L + \varepsilon}. \tag{10}$$

According to the luminance statistical characteristics, the CLAHE clip limit parameter is designed in an adaptive form:

$$C_{\mathrm{adp}} = C_{\max} - (C_{\max} - C_{\min})\eta_L, \tag{11}$$

where $C_{\mathrm{adp}}$ is the adaptive CLAHE clip limit parameter, and $C_{\min}$ and $C_{\max}$ denote the minimum and maximum values of the clip limit parameter, respectively. It can be seen from the above formula that $C_{\mathrm{adp}}$ is no longer a fixed value, but is automatically determined by the luminance fluctuation coefficient $\eta_L$ of the current image. When the luminance fluctuation is small, $\eta_L$ is small and $C_{\mathrm{adp}}$ approaches $C_{\max}$, so the enhancement intensity is relatively large, which is beneficial for improving the difference between the blue target and the background under weak-contrast conditions. When the luminance fluctuation is large, $\eta_L$ is large and $C_{\mathrm{adp}}$ approaches $C_{\min}$, so the enhancement intensity is reduced, thereby decreasing the risk of over-enhancing local strong-light, reflection, and shadow regions. Applying adaptive CLAHE enhancement to the blue response feature map $B_r$ yields the enhanced blue feature map:

$$B_e = \mathrm{CLAHE}(B_r, C_{\mathrm{adp}}), \tag{12}$$

where $B_e$ denotes the blue response feature after local contrast enhancement. This step can enhance the local difference between the blue ball and the background and improve the separability of target edges under weak-light and shadow conditions.

### 3.4. Multi-feature fusion model

When segmentation depends only on a single $b$ channel or blue response feature, it is easily affected by reflection, highlight regions, and background noise. To further improve the stability of target recognition, this paper fuses the enhanced blue feature, chromaticity feature, and luminance constraint feature to construct a comprehensive feature map.

The enhanced blue feature is used to highlight the blue target region, the chromaticity feature is used to describe the color intensity of pixels in the LAB space, and the luminance constraint term is used to suppress false detections caused by local strong light and reflection. To eliminate dimensional differences among different features, all features are normalized before fusion. The fused feature map is defined as

$$F(x,y) = \alpha B_e^n(x,y) + \beta C^n(x,y) + \gamma\left[1 - L^n(x,y)\right], \qquad \alpha+\beta+\gamma = 1, \tag{13}$$

where $B_e^n$ denotes the normalized enhanced blue feature, $C^n$ denotes the normalized LAB chromaticity feature, $L^n$ denotes the normalized luminance feature, and $\alpha$, $\beta$, and $\gamma$ are the corresponding feature weight coefficients. Through this fusion strategy, the algorithm can highlight the blue target region while suppressing the influence of local highlights and background interference on segmentation results.

The selection of the weight coefficients follows the principle of balancing target enhancement and interference suppression. The enhanced blue feature is assigned to describe the main target response, the chromaticity feature provides auxiliary color discrimination, and the luminance constraint is used to reduce false responses caused by highlights and reflections. In implementation, the coefficients are adjusted under the constraint $\alpha + \beta + \gamma = 1$ according to preliminary image observations, so that the fused feature map preserves the target boundary while avoiding excessive response in non-target bright regions.

### 3.5. Adaptive threshold segmentation and morphological processing

After the fused feature map $F$ is obtained, binary segmentation is further required. Since a fixed threshold has poor adaptability under different illumination conditions, this paper adopts an adaptive threshold method based on the statistical information of the fused feature map. Let the mean and standard deviation of the fused feature map be $\mu_F$ and $\sigma_F$, respectively. The adaptive threshold segmentation can be expressed as

$$T_{\text{adp}} = \mu_F + k\sigma_F, \qquad M_0(x,y) = \begin{cases} 1, & F(x,y) \geq T_{\text{adp}}, \\ 0, & F(x,y) < T_{\text{adp}}, \end{cases} \tag{14}$$

where $T_{\text{adp}}$ is the segmentation threshold, $k$ is the threshold adjustment coefficient, and $M_0$ is the initial binary segmentation result. Since the initial segmentation result may contain small-area noise, broken edges, or holes inside the target region, morphological opening and closing operations are further used for post-processing. Opening is used to remove small-area noise, while closing is used to connect broken edges and fill holes inside the target region. After morphological processing, a more complete and stable target region can be obtained.

### 3.6. Connected-component filtering and target center localization

After the binary segmentation result is obtained, a small number of false background regions may still exist. To remove invalid regions, connected-component analysis is performed on the binary image, and the connected region with a relatively large area and a shape consistent with ball features is selected as the target region. Then, image moments are used to calculate the target center coordinates:

$$x_c = \frac{m_{10}}{m_{00}}, \qquad y_c = \frac{m_{01}}{m_{00}}, \tag{15}$$

where $m_{00}$, $m_{10}$, and $m_{01}$ denote the zero-order and first-order moments of the target binary region, respectively, and $(x_c, y_c)$ denotes the center position of the blue ball in the image coordinate system. This coordinate can be used as the visual input for target judgment, delivery timing determination, and actuator control in the robot control module. The visualization of the recognition process is shown in Fig. 5.

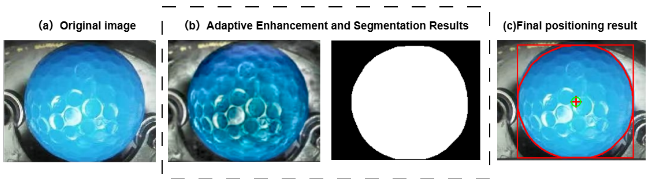


**Fig. 5.** Visualization of the blue target recognition process.

## 4. Experimental results and analysis

### 4.1. Experimental platform and settings

To verify the effectiveness of the proposed structure and algorithm, a robot intelligent delivery experimental platform was built, as shown in Fig. 1. The experimental objects were balls with a diameter of 42 mm, and the storage bin could hold up to 10 balls in a single round. The visual algorithm collected images under different illumination conditions for recognition, and the recognition results were used for robot delivery control. The experiments mainly evaluated color recognition performance, the effectiveness of the anti-jamming structure, and the continuous delivery success rate. Obstacle avoidance and other functions were also tested.

### 4.2. Comparative color recognition experiments under different illumination conditions

To analyze the adaptability of the proposed algorithm to complex illumination, normal-light, weak-light, and strong-light experimental scenarios were set up. The experiments mainly focused on target-region integrity, background false segmentation, and center localization stability. If the proposed algorithm can still maintain high F1-score and IoU under weak-light and non-uniform illumination conditions, and its Precision and Recall are better than those of other algorithms, it can be indicated that the CLAHE-LAB feature fusion strategy has good robustness to illumination changes. According to the data in Table **??**, the proposed algorithm outperforms the other algorithms under different illumination conditions, which further demonstrates its robustness to illumination variation.

During actual robot operation, external illumination is easily affected by venue lighting, shadow occlusion, and reflection from the ball surface. To improve the illumination stability of the visual acquisition area, a light shield and an auxiliary light source were installed in the robot recognition area. Under this practical supplementary-illumination condition, different color recognition algorithms were compared, further verifying the recognition stability and engineering applicability of the proposed algorithm.

### 4.3. Jamming test description and multi-color applicability

To further evaluate the structural reliability of the delivery mechanism, jamming tests were carried out under different operating conditions, including different numbers of balls in the storage bin, repeated continuous delivery cycles, and varying ball entry states. These conditions were selected because ball-bin jamming is strongly related to local accumulation, random contact, and bridge formation near the discharge channel. During the tests, the multi-hole inlet dispersed the ball entry positions, while the inner-wall limiting ribs disturbed the local support state above the discharge area. Compared with a concentrated inlet form, the proposed structure reduced the probability of stable stacking and helped maintain a more continuous discharge process.

For multi-color target recognition, the proposed framework does not depend on a fixed RGB threshold. The blue target experiment is used as a representative case to verify the effectiveness of luminance-chromaticity separation, adaptive enhancement, and feature fusion. For red, yellow, green, and white targets, the corresponding color response feature can be reconstructed from the LAB chromatic channels or combined color saliency terms, while the subsequent adaptive thresholding, morphological processing, connected-component filtering, and center localization steps remain the same. Therefore, the method has potential extensibility for multi-color delivery tasks without changing the overall control process.

## 5. Conclusion

This paper proposes a robot intelligent delivery scheme combining structural constraints and visual enhancement to improve color recognition stability and reduce ball-bin jamming during continuous multi-ball delivery. A passive anti-jamming storage structure is designed using a top light shield, multi-hole dispersed inlet array, and inner-wall limiting ribs to reduce illumination interference, local accumulation, and multi-ball bridging. Meanwhile, an adaptive CLAHE-LAB spatial feature fusion algorithm is developed to enhance blue target segmentation under complex illumination by combining luminance-chromaticity separation, local contrast enhancement, and color saliency fusion. Experimental results show that the proposed method improves recognition robustness and continuous delivery reliability. Future work will focus on three aspects: optimizing adaptive parameter selection through larger illumination datasets, extending the color response model to multi-color recognition, and integrating path planning with dynamic delivery control to improve the overall task capability of the robot in more complex environments.

## 6. Acknowledgment

This research was funded by the Fundamental Scientific Research Expenses for the Universities of Liaoning Province, grant numbers LJ212410144022, LNYJG2023077 and LJ232410144074, and project number 2025-MSLH-589.

## References


[1] V. D. Cong, L. D. Hanh, L. H. Phuong, and D. A. Duy, (2022) *"Design and development of robot arm system for classification and sorting using machine vision"* **FME Transactions *50***(1): 181–189. DOI: 10.5937/fme2201181C.

[2] S. Sanwar and M. I. Ahmed, (2023) *"Automated object sorting system with real-time image processing and robotic gripper mechanism control"* **Journal of Engineering Advancements *4***(03): 70–79. DOI: 10.38032/jea.2023.03.003.

[3] Y. Luo. "Research on Sorting System of Industrial Robot Based on Machine Vision". In: *2024 International Conference on Power, Electrical Engineering, Electronics and Control (PEEEC)*. 2024, 270–274. DOI: 10.1109/PEEEC63877.2024.00055.

[4] S. E. Schrøder, U. L. Christensen, M. H. Lauritsen, A. L. Enevoldsen, A. F. Mikkelstrup, and M. Kristiansen. "Object detection and colour evaluation of multicoloured waste textiles using machine vision". In: *Proceedings of the 16th International Conference on PErvasive Technologies Related to Assistive Environments (PETRA 2023)*. 2023, 543–549. DOI: 10.1145/3594806.3596583.

[5] I. Alrushidy, Y. Bahumid, R. Bin Shujaa, A. Abdullah, A. Kurd, and M. Abdullah, (2025) *"Design And Fabrication of Color Sorting Machine Based on Computer Vision"* **Journal of Science and Technology** ***30***(6): 107–115. DOI: 10.20428/jst.v30i6.2954.

[6] X. Tian, J. Ke, W. Wu, and J. Teng, (2025) *"Design of a Pill-Sorting and Pill-Grasping Robot System Based on Machine Vision"* **Future Internet** ***17***(11): 501. DOI: 10.3390/fi17110501.

[7] D. Giuliani, (2022) *"Metaheuristic Algorithms Applied to Color Image Segmentation on HSV Space"* **Journal of Imaging** *8*(1): 6. DOI: 10.3390/jimaging8010006.

[8] Y. S. Alsahafi, D. S. Elshora, E. R. Mohamed, and K. M. Hosny, (2023) *"Multilevel threshold segmentation of skin lesions in color images using Coronavirus Optimization Algorithm"* **Diagnostics** ***13***(18): 2958. DOI: 10.3390/diagnostics13182958.

[9] A. R. Robertson, (1977) *"The CIE 1976 color-difference formulae"* **Color Research & Application** **2**(1): 7–11. DOI: 10.1002/j.1520-6378.1977.tb00104.x.

[10] I. A. P. F. Imawati, M. Sudarma, I. K. G. Darma Putra, and I. P. A. Bayupati. "A Study of Lab Color Space and Its Visualization". In: *Proceedings of the First International Conference on Applied Mathematics, Statistics, and Computing (ICAMSAC 2023)*. 2024, 17–28. DOI: 10.2991/978-94-6463-413-6_3.

[11] C. Castiello, N. Del Buono, and F. Esposito, (2024) *"Novel color space representation extracted by NMF to segment a color image"* **Journal of Computational Mathematics and Data Science** ***13***: 100104. DOI: 10.1016/j.jcmds.2024.100104.

[12] S. M. Pizer, E. P. Amburn, J. D. Austin, R. Cromartie, A. Geselowitz, T. Greer, B. M. ter Haar Romeny, J. B. Zimmerman, and K. J. Zuiderveld, (1987) *"Adaptive histogram equalization and its variations"* **Computer Vision, Graphics, and Image Processing** ***39***(3): 355–368. DOI: 10.1016/S0734-189X(87)80186-X.

[13] J. Guo, J. Ma, Á. F. García-Fernández, Y. Zhang, and H. Liang, (2023) *"A survey on image enhancement for low-light images"* **Heliyon** ***9***(4): e14558. DOI: 10.1016/j.heliyon.2023.e14558.

[14] J. Zhan, E. S. Goh, and M. S. Sunar, (2024) *"Low-light image enhancement: A comprehensive review on methods, datasets and evaluation metrics"* **Journal of King Saud University - Computer and Information Sciences** ***36***(10): 102234. DOI: 10.1016/j.jksuci.2024.102234.

[15] Y. Demir and N. H. Kaplan, (2023) *"Low-light image enhancement based on sharpening-smoothing image filter"* **Digital Signal Processing** ***138***: 104054. DOI: 10.1016/j.dsp.2023.104054.

[16] Y. Cai, H. Bian, J. Lin, H. Wang, R. Timofte, and Y. Zhang. "Retinexformer: One-stage Retinex-based Transformer for low-light image enhancement". In: *Proceedings of the IEEE/CVF International Conference on Computer Vision (ICCV)*. 2023, 12470–12479. DOI: 10.1109/ICCV51070.2023.01149.

[17] T. Wang, K. Zhang, T. Shen, W. Luo, B. Stenger, and T. Lu. "Ultra-high-definition low-light image enhancement: A benchmark and transformer-based method". In: *Proceedings of the AAAI Conference on Artificial Intelligence*. **37**. 3. 2023, 2654–2662. DOI: 10.1609/aaai.v37i3.25364.

[18] X. Xu, R. Wang, C. W. Fu, and J. Jia. "SNR-Aware Low-Light Image Enhancement". In: *Proceedings of the IEEE/CVF Conference on Computer Vision and Pattern Recognition (CVPR)*. 2022, 17693–17703. DOI: 10.1109/CVPR52688.2022.01719.

[19] L. Ma, T. Ma, R. Liu, X. Fan, and Z. Luo. "Toward Fast, Flexible, and Robust Low-Light Image Enhancement". In: *Proceedings of the IEEE/CVF Conference on Computer Vision and Pattern Recognition (CVPR)*. 2022, 5627–5636. DOI: 10.1109/CVPR52688.2022.00555.

[20] S. Qiao and R. Chen, (2024) *"Progressive feature fusion for SNR-aware low-light image enhancement"* **Journal of Visual Communication and Image Representation** ***100***: 104148. DOI: 10.1016/j.jvcir.2024.104148.

[21] H. Zhang, L. Wang, Q. Zou, and J. Zeng, (2025) *"DFFNet: Deep Feature Fusion Network for low-light image enhancement"* **Image and Vision Computing** ***161***: 105645. DOI: 10.1016/j.imavis.2025.105645.

[22] D. Gella, D. Maza, and I. Zuriguel, (2022) *"On the dual effect of obstacles in preventing silo clogging in 2D"* **Communications Physics** ***5***: 4. DOI: 10.1038/s42005-021-00756-4.

[23] S. Zhang, Z. Zeng, H. Yuan, Z. Li, and Y. Wang, (2024) *"Precursory arch-like structures explain the clogging probability in a granular hopper flow"* **Communications Physics** ***7***: 202. DOI: 10.1038/s42005-024-01694-7.